OXFORD

Human Molecular Genetics, 2017, Vol. 26, No. 22 4327–4339

doi: 10.1093/hmg/ddx319
Advance Access Publication Date: 24 August 2017
Original Article

ORIGINAL ARTICLE

Retinal pigment epithelium cholesterol efflux mediated by the 18 kDa translocator protein, TSPO, a potential target for treating age-related macular degeneration

Lincoln Biswas[1], Xinzhi Zhou[1], Baljean Dhillon[2], Annette Graham[1] and Xinhua Shu[1,*]

[1]Department of Life Sciences, Glasgow Caledonian University, Glasgow G40BA, UK and [2]Centre for Clinical Brain Sciences, University of Edinburgh, Edinburgh EH16 4SB, UK

*To whom correspondence should be addressed. Tel: +44 1413318763; Fax: +44 141 3313208; Email: xinhua.shu@gcu.ac.uk

Abstract

Cholesterol accumulation beneath the retinal pigment epithelium (RPE) cells is supposed to contribute the pathogenesis of age-related macular degeneration (AMD). Cholesterol efflux genes (*APOE* and *ABCA1*) were identified as risk factors for AMD, although how cholesterol efflux influences accumulation of this lipid in sub-RPE deposits remains elusive. The 18 kDa translocator protein, TSPO, is a cholesterol-binding protein implicated in mitochondrial cholesterol transport. Here, we investigate the function of TSPO in cholesterol efflux from the RPE cells. We demonstrate in RPE cells that TSPO specific ligands promoted cholesterol efflux to acceptor (apo)lipoprotein and human serum, while loss of TSPO resulted in impaired cholesterol efflux. *TSPO*$^{-/-}$ RPE cells also had significantly increased production of reactive oxygen species (ROS) and upregulated expression of proinflammatory cytokines (IL-1β and TNFα). Cholesterol (oxidized LDL) uptake and accumulation were markedly increased in *TSPO*$^{-/-}$ RPE cells. Finally, in aged RPE cells, TSPO expression was reduced and cholesterol efflux impaired. These findings provide a new pharmacological concept to treat early AMD patients by stimulating cellular cholesterol removal with TSPO specific ligands or by overexpression of TSPO in RPE cells.

Introduction

Age-related macular degeneration (AMD) is the commonest cause of registered blindness in the developed world (1). An important clinical feature of AMD is the accumulation of both focal (Drusen) and diffuse extracellular (basal) deposits in the macula, between the retinal pigment epithelium (RPE) and the adjacent Bruch's membrane. One current hypothesis is that these deposits lead to dysfunction and later death of RPE and associated loss of photoreceptors (2). Ageing is associated with progressive accumulation of lipids within Bruch's membrane (3). Lipid deposition causes hydraulic conductivity and macromolecular permeability in Bruch's membrane, which is thought to impair retinal metabolism. Histopathological analyses of AMD patients' eyes have demonstrated the presence of apolipoproteins, cholesterol and cholesteryl ester deposits underneath the RPE, implicating abnormal cholesterol transport in the progression of this disease (4). Genome wide association studies have also implicated that hepatic lipase C (*LIPC*) and cholesteryl ester transfer protein (*CETP*), key genes involved in the metabolism of triglycerides and high-density lipoproteins (HDL), in the pathogenesis of AMD (5,6).

Excess cholesterol is removed from peripheral cells by the reverse cholesterol transport (RCT) pathway, by which HDL return excess cellular cholesterol to the liver for either storage as

Received: July 13, 2017. **Revised:** August 3, 2017. **Accepted:** August 6, 2017

cholesteryl ester droplets or for excretion in bile. Cholesterol efflux is the first step in RCT mediated by the removal of cholesterol by acceptors, such as (apo)lipoproteins. Cholesterol efflux is mediated by ATP-binding cassette (ABC) transporters, such as ABCA1, ABCG1 and ABCG4 (7). Our previous work in human macrophages has established that increased mitochondrial cholesterol trafficking, via the 18 kDa translocator protein (TSPO), can enhance expression of key genes encoding proteins involved in the cholesterol efflux pathway, and facilitate removal of cholesterol by apolipoprotein acceptors (8). Transfer of cholesterol to mitochondrial sterol 27-hydroxylase (CYP27A1) increases generation of oxysterol ligands for Liver X receptors, which induce the expression of ABCA1, ABCG1/4 and ApoE.

Mitochondrial cholesterol trafficking is thought to involve a complex of proteins including TSPO, steroidogenic acute regulatory protein (StAR), the voltage dependent anion channel (VDAC) and possibly the adenine nucleotide channel (ANC), together with putative regulatory proteins (9). The TSPO protein, previously called the peripheral-type benzodiazepine receptor, is an 18 kDa transmembrane protein localized in the outer mitochondrial membrane of different tissues. TSPO is thought to mediate a number of functions, including cholesterol transport, steriodogenesis, neuroinflammation, prevention of apoptosis and stress adaption (9). Global or conditional *Tspo* knockout (KO) mouse models have been reported; the KO mice exhibited divergent phenotypes (embryonic lethal, defect in steroidogenesis, or no effect on steroidogenesis) possibly due to genetic background differences between strains of those KO mice (10–12).

The RCT process may be important in the pathogenesis of AMD because of its involvement in lipid and cholesterol transport from RPE (13). The RPE cells are involved in phagocytosis and degradation of photoreceptor outer segments (POS), which are thought to be the major source of excess RPE lipids. Incompletely digested POS lipids accumulate as autofluorescent lipid-protein aggregates called lipofuscin in RPE. Retinoid metabolites, such as bis-retinoids, also contribute to the formation of lipofuscin (14). About 20% of RPE cell volume is occupied by lipofuscin by the age of 80 years (15). Notably, the lipofuscin fluorophore A2E blocks cholesterol efflux, resulting in the accumulation of both free cholesterol and cholesteryl esters in RPE cells (14). Further, RPE cells have been shown to express ABCA1, scavenger receptor BI (SR-BI), apolipoprotein A-I (ApoA-I) and apolipoprotein E (ApoE), which participate in the RCT process (16); ABCA1 and ApoE are also associated with susceptibility to AMD (6,17). ApoE is synthesized and secreted by RPE cells in considerable amounts comparable to those in the liver and brain, the two most abundant biological synthetic sources of ApoE (18). ApoE and ApoA-I proteins were detected in drusen and have been implicated in apolipoprotein-mediated RCT in lipid trafficking and in facilitating the efflux of lipids from the RPE, and their transit across Bruch's membrane to the choroidal vasculature (19).

There have been no previous studies investigating the function of the mitochondrial cholesterol trafficking protein, TSPO, in RPE cells. In this study, we found TSPO to be highly expressed in human RPE (ARPE-19 cell line) and mouse RPE cells. We also found TSPO ligands significantly increased cholesterol efflux to ApoE, ApoA-I and HDL from RPE cells. When TSPO was deleted in RPE cells, TSPO-specific ligand treatment could not increase cholesterol efflux. Aged mouse RPE cells had significantly decreased *Tspo* expression and impaired cholesterol efflux. Our observations demonstrated that TSPO is involved in regulating cholesterol efflux from RPE cells, suggesting TSPO as a potential therapeutic target for AMD.

Results

TSPO ligands increased cholesterol efflux from RPE cells

Previously reports showed that TSPO, a mitochondrial outer membrane protein, is expressed in fibroblasts, macrophages, microglia and astrocytes (8,20–25). We examined TSPO expression in ARPE-19 cells using a rabbit monoclonal antibody and found TSPO to be present and localized to mitochondria (Fig. 1). Initially, human ARPE-19 cells were treated with a range of TSPO ligands at different concentrations (2.5–30 μM), compared with the vehicle control, to determine the highest concentration that does not significantly affect the viability of ARPE-19 cells over 24 h treatment. The suitable concentration of each ligand was identified as FGIN-1-27 (10 μM), XBD173 (25 μM) and Etifoxine (20 μM) respectively (Supplementary Material, Fig. S1).

Previous reports demonstrated that TSPO regulated cholesterol efflux in fibroblast and macrophage cells (8,21). We treated ARPE-19 cells with TSPO specific ligands for 24 h and found that FGIN-1-27 and XBD173 significantly increased cholesterol efflux to apoE, apoA-I, HDL and human serum (HS), and Etifoxine significantly increased cholesterol efflux to HDL and HS (Fig. 2).

Ligands of TSPO decreased lipogenesis in RPE cells

We investigated whether treatment of TSPO ligand affected lipogenesis in ARPE-19 cells by measuring the syntheses of phospholipid, triacylglycerol, cholesteryl and fatty acid. We found significantly reduced incorporation of [^{14}C]acetate into phospholipid by 30% in FGIN-1-27 treated cells and by 36% in XBD173 treated cells. Incorporation of [^{14}C]acetate into free cholesterol pools was also significantly decreased by 35% in FGIN-1-27 treated cells and by 31.52% in XBD173 treated cells, compared with the vehicle control (Fig. 3A, B). By contrast, there was no significant difference when incorporation of [^{14}C]acetate into triglycerides, fatty acid and cholesterol ester pools between ligand-treated and control cells were compared (Fig. 3A, B). Etifoxine-treated ARPE-19 cells exhibited significant reduction by 57.42% in incorporation of [^{14}C]acetate into the free cholesterol pool compared with the vehicle control; the other examined lipid pools showed no significant changes for the same comparison (Fig. 3C). We also measured total cholesterol mass and phospholipids in control and ligand treated ARPE-19 cells and found significant reduction in total cholesterol by 35.49, 32.51 and 23.61% in FGIN-1-27, XBD173 and Etifoxine treated cells, respectively (Fig. 3D) and in phospholipid contents by 29.18 and 9.93% in FGN1-27 and XBD173 treated cells respectively (Fig. 3E).

Ligands of TSPO increased gene expression of proteins involved in cholesterol transport and metabolism in RPE cells

Since treatment with TSPO ligands influenced cholesterol efflux (Fig. 2), we examined expression of genes involved in cholesterol homeostasis in ARPE-19 cells that were treated with FGIN-1-27 (10 μM), XBD173 (25 μM) or Etifoxine (20 μM) for 24 h. The mRNA expression levels of these genes relative to housing keeping gene *GAPDH* were shown in Supplementary Material, Figure S2A. FGIN-1-27 significantly upregulated the expression of *NR1H3* (encoding to liver X receptor alpha protein, LXRα), *ABCA1*, *ABCG1* and *CYP27A1* but not *CYP46A1* (Supplementary Material, Fig. S2A), while Etifoxine notably enhanced the expression of *LXRα*, *ABCA1*, *ABCG1* and *CYP46A1* except *CYP27A1*

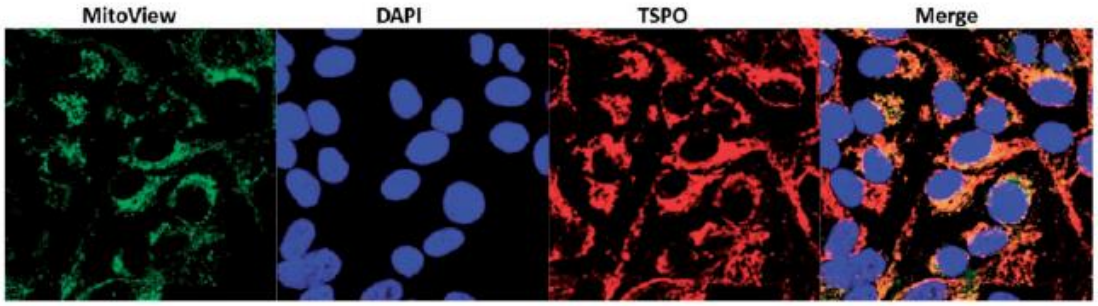

Figure 1. TSPO localization in ARPE-19 cells. ARPE-19 cells were incubated with MitoView (mitochondria marker) and fixed with cold methanol, then incubated with anti-TSPO antibody and secondary antibody. TSPO was cololcalized with MitoView in mitochondria.

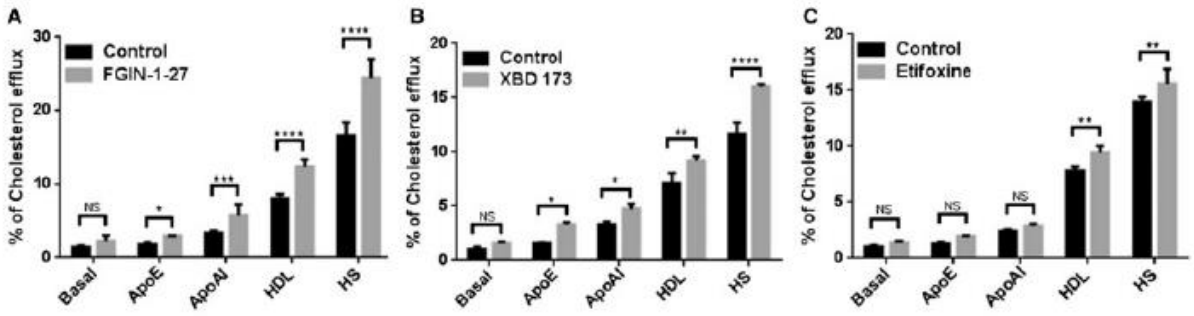

Figure 2. Cholesterol acceptor-mediated cholesterol efflux was measured from ARPE-19 cells. The cells were treated with TSPO ligand, FGIN-1-27 (10 μM), XBD137 (25 μM) or Etifoxine (20μM) for 24 h. The percentage of [^{3}H] cholesterol efflux was measured from the medium and the cellular lipids. Data was presented as means ± SD. Every experiment was performed in triplicate and three independent experiments were carried out. NS: non-significant, *P < 0.05, **P < 0.01, ****P < 0.0001.

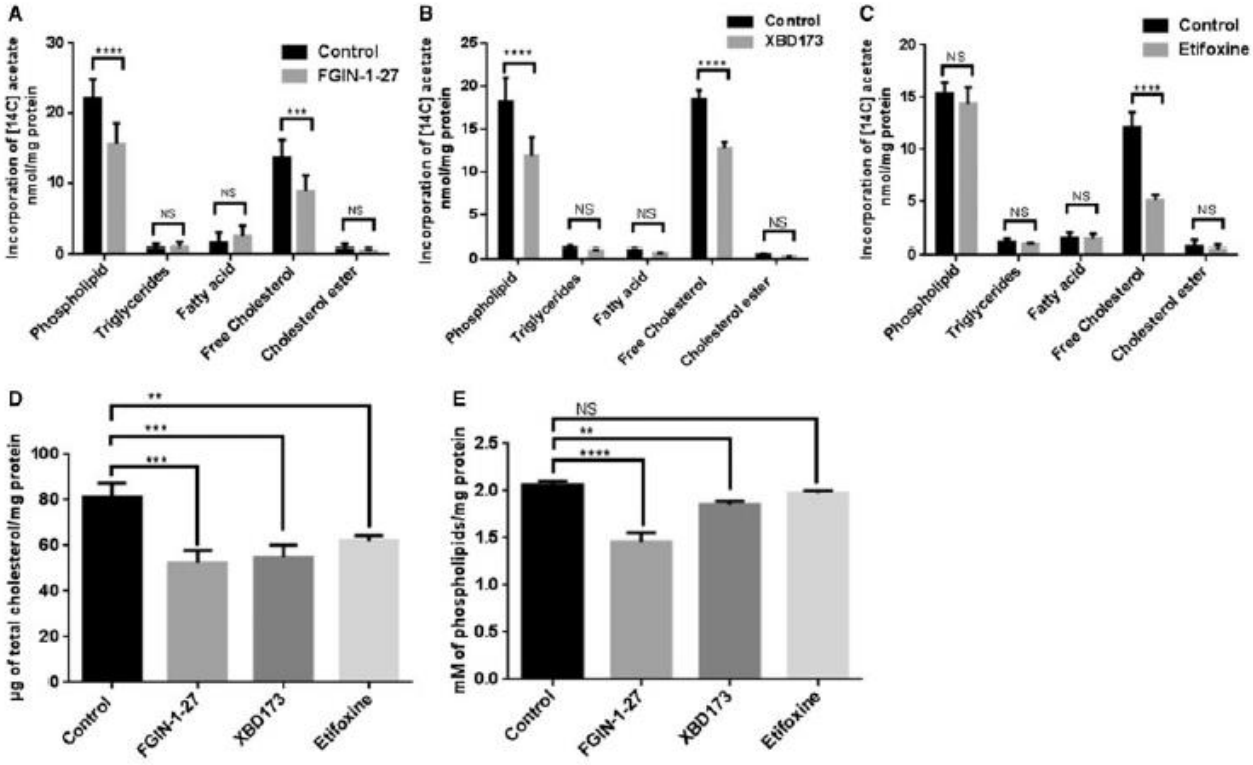

Figure 3. TSPO ligand modulation of lipids phenotypes. A–C Impact of TSPO ligands (Fgin-1-27, XBD173 and Etifoxine) on nmol incorporation per mg total protein of [^{14}C] acetate (1 μCi/ml) into phospholipid, triacylglycerol, cholesteryl ester, free cholesterol and fatty acid pools compared with the vehicle control. The incorporation of radiolabel was normalized to mg total cellular protein. The effect of TSPO ligands on the ARPE-19 total cholesterol (D) and phospholipids mass (E) were reduced significantly due to expose to TSPO ligands for 24 h. Values of total cholesterol and phospholipids from above experiments were normalized based on total cellular protein. Three independent experiments were performed. **P < 0.01, ***P < 0.001, ****P < 0.0001.

(Supplementary Material, Fig. S2A). XBD173 significantly increased expression of all examined genes when compared to the vehicle controls (Supplementary Material, Fig. S2A). We also assessed protein levels of LXRα, ABCG1, ABCA1, CYP27A1 and CYP46A1 in ARPE-19 treated with TSPO ligands, by Western blotting (Supplementary Material, Fig. S2B). FGIN-1-27 treatment resulted in significant increases of LXRα, ABCG1 and ABCA1 proteins, compared with the vehicle controls, but the trend towards increased expression of CYP27A1 and CYP46A1 proved non-significant (Supplementary Material, Fig. S2C). Etifoxine treatment caused notable increases in expression of ABCG1 and CYP46A1 protein, but no significant increases in LXRα, ABCA1and CYP27A1 proteins were observed, compared with the vehicle controls (Supplementary Material, Fig. S2C). Incubation with XBD173 significantly increased the levels of LXRα, ABCG1, CYP27A1 and CYP46A1 proteins, but did not significantly alter the levels of ABCA1 protein (Supplementary Material, Fig. S2C).

Knockout of TSPO in RPE cells using the CRISPER/Cas9 engineering system

Human TSPO gene contains four exons with exon 1 untranslated (Fig. 4A). To delete TSPO, we followed the protocol of the CRISPR/Cas9 system and designed a guide RNA (gRNA) having sequence complementary to 18 nucleotides (c.87_104) of TSPO exon 2 (Fig. 4A). ARPE-19 cells were transfected with the gRNA construct and the Cas9 expression plasmid. Nine colonies were derived from G418 transient selection. Two colonies, named KO1 and KO2, with loss of TSPO were confirmed by Western blotting using a TSPO-specific antibody (Fig. 4B). Immunocytochemistry further confirmed TSPO was absent from KO1 and KO2 cells (Fig. 4C). We used Sanger Sequencing to find that KO1 had an insertion of 82 bp (cc.101_102ins82.) and KO2 contained a deletion of 8 bp (c.96_103del8) in the target region of exon 2 (Fig. 4A). The deletion/insertion mutations resulted in frame-shift reading with truncated peptides (Supplementary Material, Fig. S3).

Increased lipid accumulation in TSPO knockout RPE cells

Treatment with TSPO specific ligands enhanced cholesterol efflux in ARPE-19 cells (Fig. 2). However, when TSPO was deleted, the knockout cells had no significant change in [^{3}H]cholesterol efflux to apoE, apoA-I, HDL, or human serum after treatment with FGIN-1-27, XBD173 or Etifoxine (Supplementary Material, Fig. S4). We therefore investigated whether loss of TSPO in APRE-19 cells cause lipid accumulation. When wildtype and

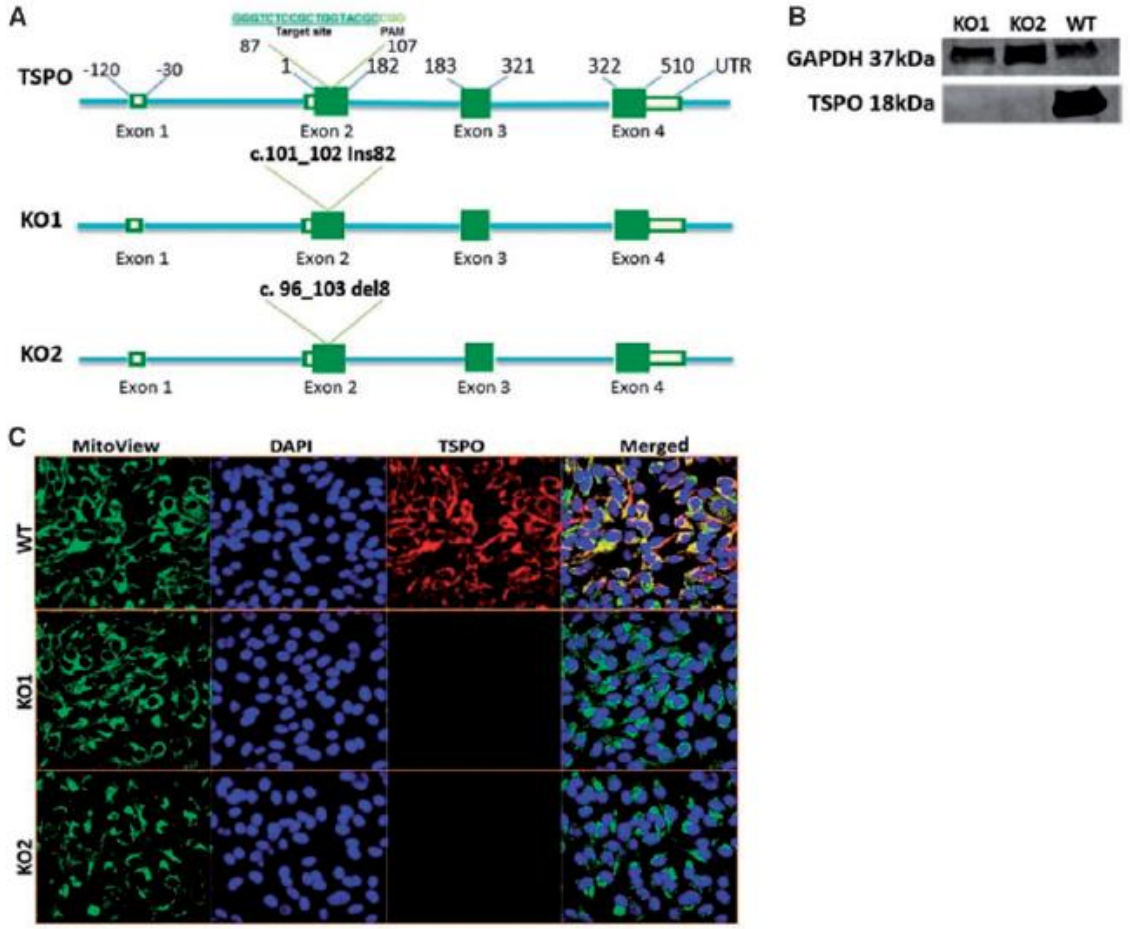

Figure 4. CRISPR/Cas9 system mediated knockout of TSPO from ARPE-19 cells. (A) Schematic structure of TSPO gene, the targeting sequence and the protospacer adjacent motif (PAM) were shown. (B) After transfection with TSPO-CRISPR/Cas9 construct, ARPE-19 colonies were screened for TSPO protein expression using a monoclonal TSPO antibody. Two TSPO-deleted colonies (KO1 and KO2) were identified by Western blotting. (C) Immunocytochemistry also confirmed the complete absence of TSPO from mitochondria (MitView Green) in knockout ARPE-19 cells.

TSPO$^{-/-}$ cells were incubated with DiI-OxLDL for 24 h we found intracellular OxLDL were significantly increased in TSPO$^{-/-}$ cells by 39% ($P < 0.01$) compared to wildtype cells (Fig. 5A, B). We also confirmed significant increase of OxLDL accumulation in TSPO deleted RPE cells using fluorescence-activated cell sorting assay (Fig. 5C) .We determined whether the increase of OxLDL accumulation was also related oxLDL uptake in TSPO$^{-/-}$ cells, we fed both wildtype and TSPO$^{-/-}$ cells with DiI-OxLDL for 4 h and assessed intracellular oxLDL by confocal imaging and FACS assay. We found that uptake of OxLDL was significantly increased by 34% in TSPO deleted cells (Fig. 5D-E).

Previous data showed uptake of LDL and OxLDL by rodent RPE cells occurs primarily via LDL receptor (LDLR) (26), which is expressed in both rodent and human RPE cells (26,27). We used qRT-PCR and Western blotting to assess the level of LDLR in wildtype and TSPO deleted cells loaded with OxLDL. The *LDLR* mRNA level in TSPO$^{-/-}$ cells incubated with oxLDL for 4 and 24 h was significantly increased by 2341 fold and 1501 fold, respectively, when compared to that of wildtype cells (Fig. 6A, C). Expression of LDLR protein also increased significantly in TSPO$^{-/-}$ cells when compared to wildtype cells (Fig. 6B, D). Intracellular OxLDL cause increased oxidative stress, promoting the production of inflammatory cytokines, IL-1β and TNFα, that enhance LDLR expression (28–30). We therefore measured reactive oxygen species (ROS) production in both wildtype and TSPO$^{-/-}$ RPE cells cultured in serum-free medium or in serum-free medium with OxLDL. When cultured in serum-free medium, TSPO$^{-/-}$ cells produced significantly higher level of ROS at 4 and 24 h by 39 and 52% respectively (Fig. 7A, B), consistent with early report that deletion of TSPO increased ROS production in steroidogenic cells (31). Both wildtype and TSPO-deleted RPE cells incubated with OxLDL had marked increase of ROS production at 4 and 24 h when compared to cells cultured in serum-free medium, indicating oxLDL promoted ROS production. In the presence of OxLDL, TSPO$^{-/-}$ cells also had significant increase of ROS production when compared to wildtype RPE cells at 4 and 24 h by 64 and 58% respectively (Fig. 7A, B).

We also measured the secretion of IL-1β and TNFα into the media above wildtype and TSPO-deleted cells by enzyme-linked immunosorbent assay (ELISA). When cultured in serum-free medium, TSPO$^{-/-}$ cells exhibited a trend towards increased output of IL-1β at 4 and 24 h though there was no significant difference compared to wildtype cells. However, TNFα levels were increased in the media above TSPO$^{-/-}$ cells by 37%, with a

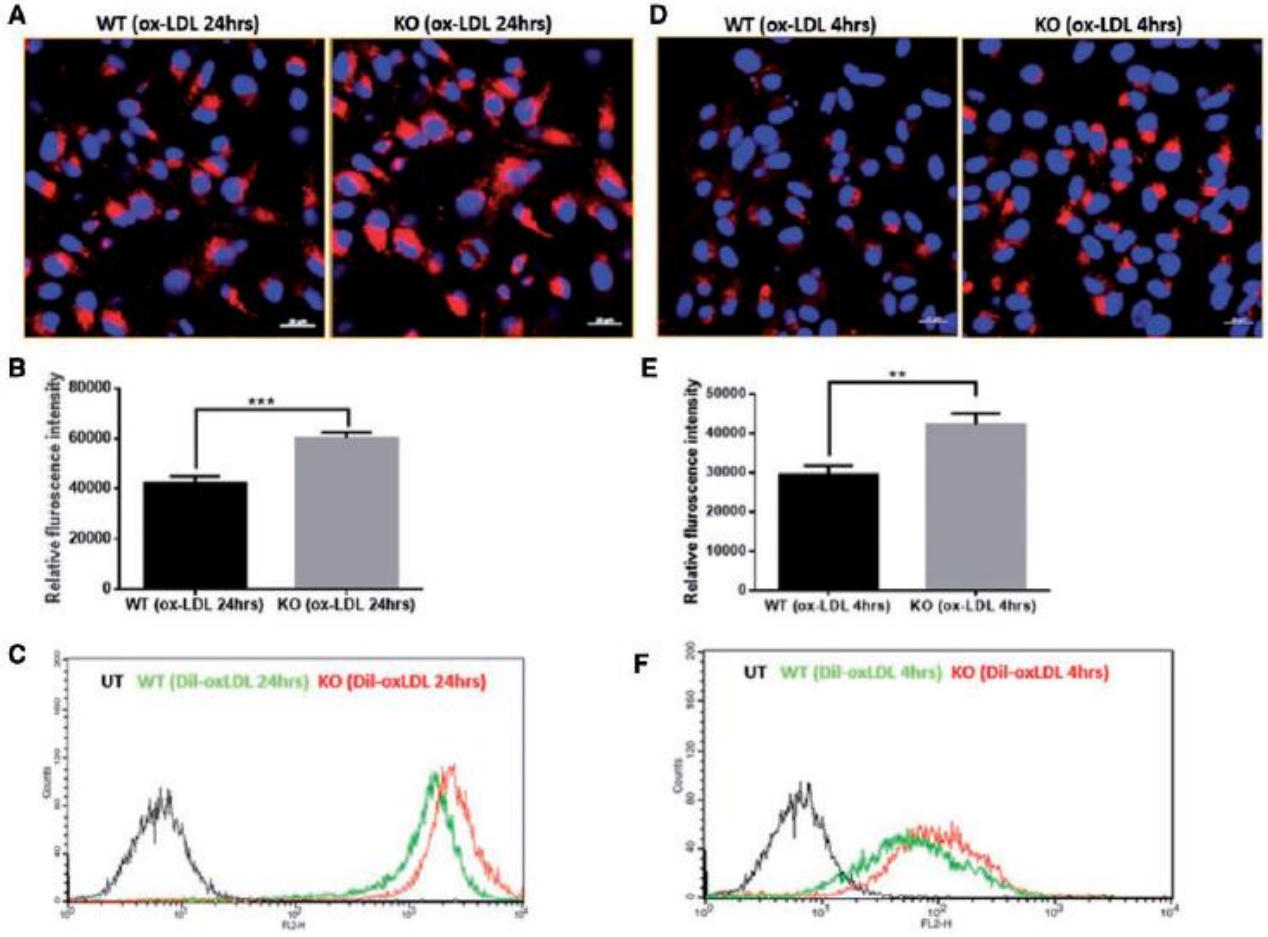

Figure 5. Significantly increased cholesterol accumulation and uptake in TSPO$^{-/-}$ cells. The wildtype and TSPO$^{-/-}$ ARPE-19 cells were incubated with DiI-oxLDLa (20 μg/ml) for 4 or 24 h. The intracellular oxLDL was detected by confocal microscopy and also assessed by fluorescence-activated cell sorting (FACS). (A) Confocal image showing more oxLDL accumulation in TSPO deleted RPE cells. (B) Quantification of fluorescence signals by using Image J software showing significant increase of oxLDL accumulation in TSPO$^{-/-}$ cells when compared to wildtype cells. (C) FACS showing significant increase of fluorescence intensity in TSPO$^{-/-}$ RPE cells when compared to the wildtype cells exposed to oxLDL for 24 h ($P < 0.001$). (D) Confocal image showing increased uptake of oxLDL. (E) Quantification of the increase using Image J software confirming the increase of uptake by 34% in TSPO knockout cells. (F) FACS showing marked increase of oxLDL uptake in TSPO-deleted cells ($P < 0.001$). **$P < 0.01$, ***$P < 0.001$.

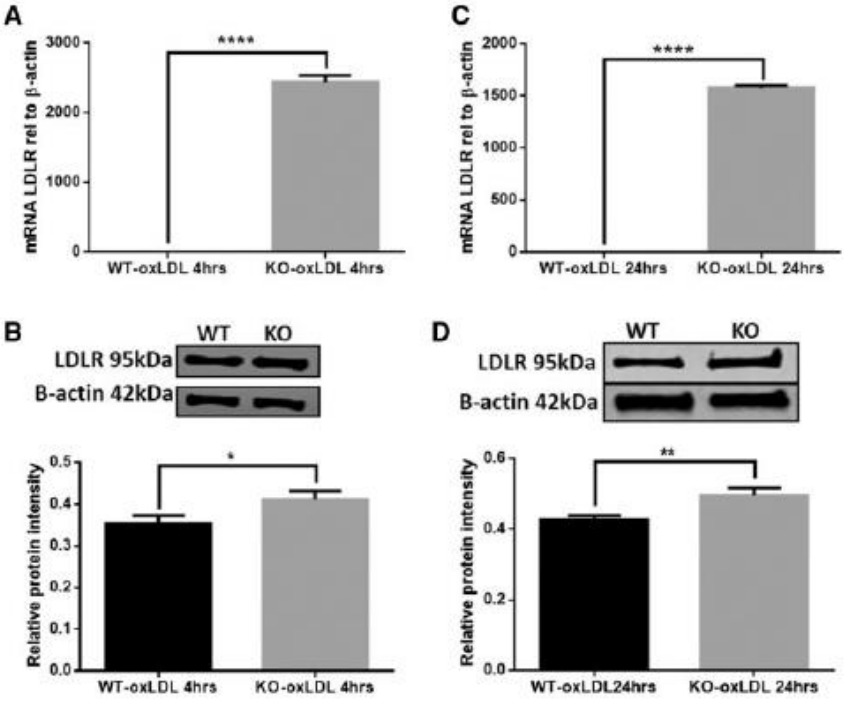

Figure 6. The expression of LDLR was quantified after exposure to oxLDL. (A) After 4 h incubated with oxLDL, mRNA level of *LDLR* was increased 2341 fold in TSPO knockout cells compared to wild type cells as well as protein level also increased significantly (B). Similarly, after 24 h incubation of oxLDL, *LDLR* mRNA (C) and protein (D) were significantly increased. Data were presented as mean ± SD. NS: no significance, * $P < 0.05$, ** $P < 0.01$, *** $P < 0.001$.

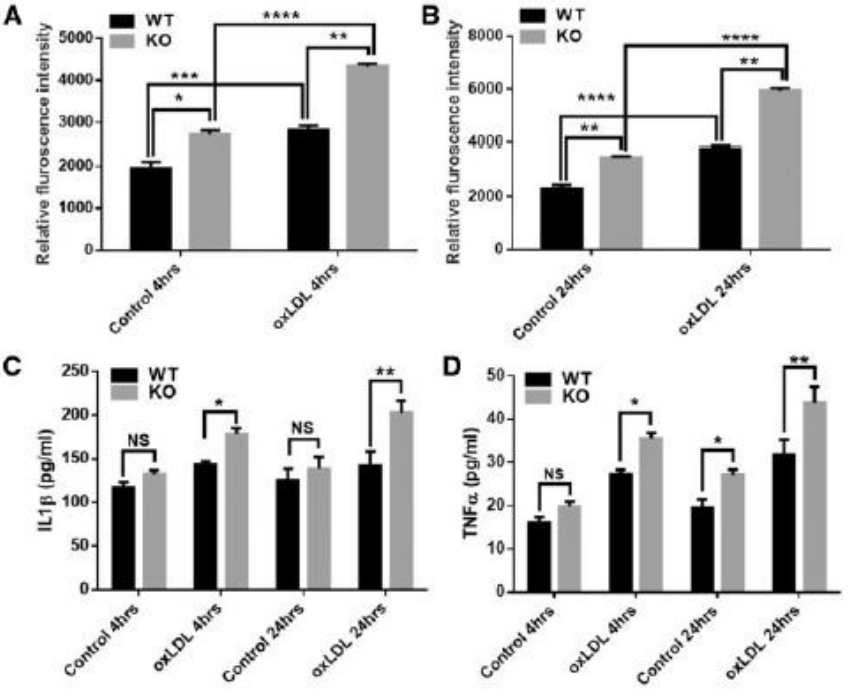

Figure 7. Significantly increased reactive oxygen species (ROS) and inflammatory cytokines levels in TSPO-deleted RPE cells. Wildtype (WT) and TSPO knockout (KO) ARPE-19 cells were exposed to oxLDL (200 μg/ml) or vehicle control for 4 or 24 h. (A) Cellular ROS levels were increased markedly after treated with oxLDL (4 h), however in TSPO-deleted cells ROS were remarkably higher than that of wildtype cells. Similarly, marked increase of ROS also occurred in TSPO knockout cells after 24 h exposure to oxLDL (B). The levels of the inflammatory cytokines (IL-1β and TNFα) were significantly increased TSPO deleted cells after exposure to oxLDL for 4 or 24 h (C, D). NS: no significance, * $P < 0.05$, ** $P < 0.01$, *** $P < 0.001$, **** $P < 0.0001$.

significant difference noted from the wildtype control at 24 h (Fig. 7C, D). Levels of both IL-1β and TNFα were markedly higher in TSPO$^{-/-}$ cells compared to wiltype cells when incubated with oxLDL at 4 and 24 h (Fig. 7C, D). Further, when wildtype and TSPO$^{-/-}$ RPE cells were treated with IL-1β (10 ng/ml) or TNFα (50 ng/ml) for 4 h, the level of LDLR protein was significantly, if modestly, increased in TSPO-deleted cells; when treated for 24 h with these cytokines, LDLR protein levels were significantly increased in both wildtype and TSPO$^{-/-}$ cells (Supplementary Material, Fig. S5).

Reduced TSPO expression and impaired cholesterol efflux in aged mouse RPE cells

Wang *et al.* (2015) examined TSPO localization in developmental and young adult mouse retina and showed TSPO was localized in the developing and migratory microglia at P0, P3 and P7, while the localization in microglia disappeared at P14. At P28 (young adult), TSPO signal was detected only in retinal blood vessels and not in any other retinal cells, however TSPO protein was gradually increased during retinal development with significant high level in young adult retina (25). We performed immunostaining to detect TSPO expression in the retinas of adult mice (3 months old) and found a marked strong signal in RPE cell layer, and quite a strong signal presented in the ganglion cell layer (Fig. 8A, B). We also detected TSPO immunopositivity in the choroid, possibly in the choroid vessels. We quantified the expression of *Tspo* mRNA and protein in mouse retina and RPE/choroid: *Tspo* mRNA level in RPE/choroid was 20.7 fold higher than that in the retina, TSPO protein level in RPE/choroid was 16.7 fold higher than that in the retina (Fig. 8C–E).

We further investigated TSPO expression in aged mouse RPE and retina: TSPO was significantly decreased by 58.67% at mRNA level and by 24.46% at protein level in 20-month old mouse RPE cells when compared to that of 3-month old RPE cells (Fig. 9A–C). Expression of the cholesterol transporter genes, *Abca1* and particularly *Abcg1*, in aged RPE was also significantly decreased (Supplementary Material, Fig. S6A). In aged mouse retina, we also detected significantly declined expression of *Tspo*, *Abca1* and *Abcg1* (Supplementary Material, Fig. S6B).

The total cholesterol mass was measured in 3-month and 20-month old mouse RPE and that the cholesterol mass of 20-month old RPE was significantly higher than that of 3 moth-old RPE/choroid (Fig. 9D). We therefore investigated whether the increase of total cholesterol in aged RPE is partially due to a defect in cholesterol efflux. We observed that the percentage of [^{3}H]cholesterol efflux to apoE, apoA-I, HDL, or human serum was significantly decreased in 20-months old RPE when compared to that of 3-months old RPE (Fig. 9E).

Discussion

Extensive clinical studies show abnormal cholesterol accumulation in drusen of AMD patients, implicating dysregulated

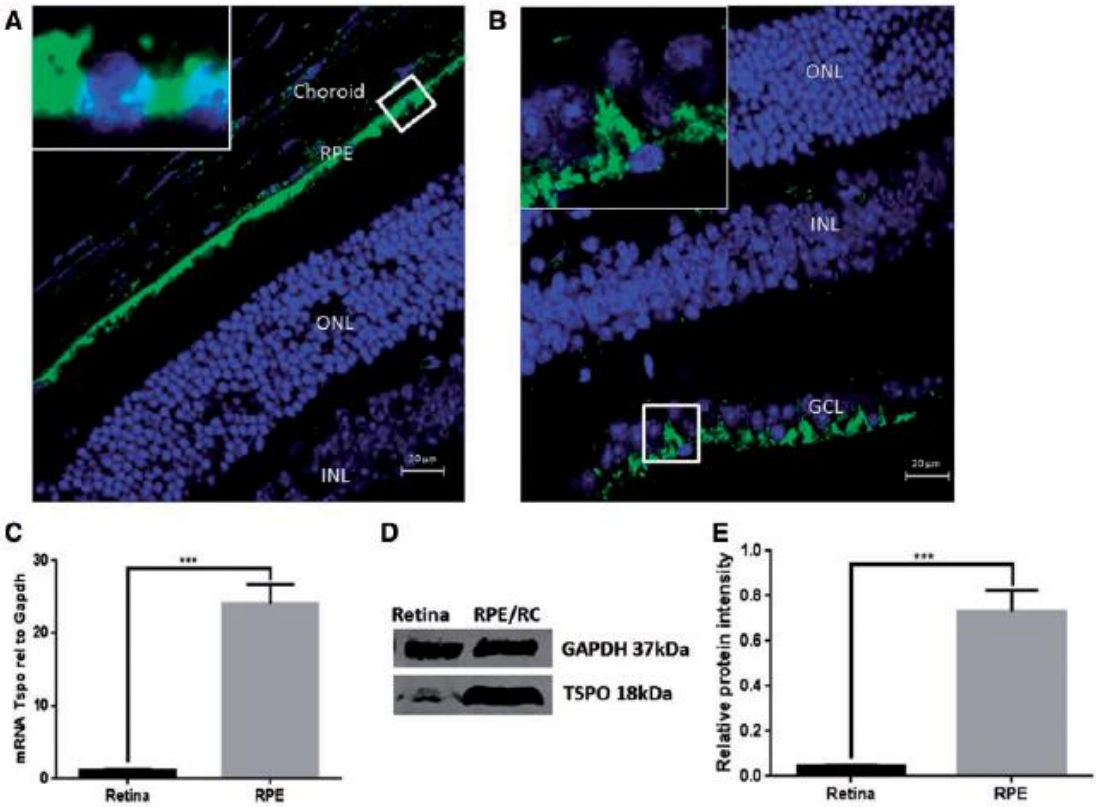

Figure 8. TSPO protein in mouse retina and RPE/choroid. Three-month old mouse eye sections were immunostained with an TSPO antibody for TSPO expression and DAPI for labelling nuclei. (A) Immunolocalization of TSPO in choroid, retinal pigment epithelium (RPE), outer nuclear layer (ONL) and inner nuclear layer (INL). Strong TSPO signals were presented in the RPE layer. (B) TSPO signals detected in ganglial cells layer (GCL). Retina and RPE/choroid (RC) were lysed to quantify TSPO expression at mRNA and protein levels. Inserts show a 4X magnification of the selected regions. Both mRNA (C) and protein (D, E) of TSPO were significantly higher in RPE/RC than that of the retina. Data were presented as mean ± SD. ***$P < 0.001$.

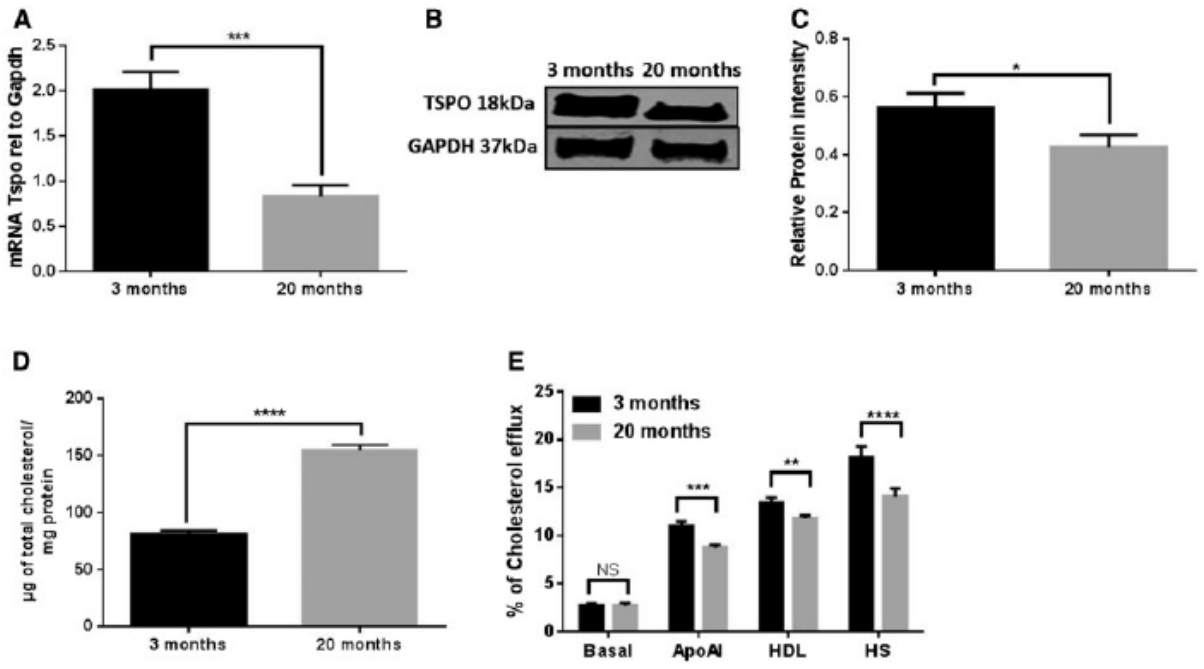

Figure 9. TSPO expression, total cholesterol and cholesterol efflux in aged mouse RPE. (**A**) mRNA of *Tspo* expression was significantly decreased in 20-month old mouse RPE cells. (**B, C**) TSPO protein in RPE cell derived from 20-month old mice was also significantly decreased. TSPO protein intensity was normalized to GAPDH. (**D**) Total cholesterol contents of RPE cells derived from 3-month or 20-month mice were measured and normalized to total protein contents. RPE cells from 20-month old mice had marked higher level of total cholesterol when compared to RPE cells form 3-month old mice. (**E**) RPE cell derived from 3 or 20months old mice were labelled with 0.5µCi/ml [^{3}H] cholesterol for 24 h followed by 24 h incubation with or without Apo A-I (10 µg/ml), HDL (20 µg/ml) and human serum (HS, 1% v/v). After incubation, the percentage of [^{3}H]cholesterol efflux was measured. RPE cells from aged (20-month old) had significant decrease in cholesterol efflux to ApoAI, HDL and human serum.

cholesterol homeostasis (32). Experimental research has demonstrated that impaired cholesterol efflux might contribute to the pathogenesis of AMD (15,33). However, the underlying mechanisms are not fully understood. The present study demonstrated that TSPO ligands enhance cholesterol efflux in RPE cells. Deletion of TSPO prevented modulation on cholesterol efflux by TSPO ligands and resulted in markedly increased cholesterol (OxLDL) uptake and accumulation in TSPO$^{-/-}$ RPE cells. Aged mice had significant decrease in retinal and RPE expression of TSPO and defective cholesterol efflux in aged primary RPE cells.

TSPO is an outer mitochondrial membrane (OMM) protein with five transmembrane (TM) helixes and can bind cholesterol at a high affinity through its C-terminal cholesterol recognition amino acid consensus (CRAC) motif to transport cholesterol to the inner mitochondrial membrane (IMM) (34,35). TSPO can also bind different ligands, which promote cholesterol movement from OMM to IMM, where cholesterol is converted into pregnenolone by CYP11A1 in steroidogenic tissues or into oxyterols (27-hydroxycholesterol and 5-cholestanoic acid) by CYP27A1 in macrophage and other cell types (34). Oxysterols can activate a nuclear transcription factor, liver X receptor (LXRα/β), thereby upregulating the transcription of ABCA1, ABCG1 and ABCG4, which promote cholesterol efflux. In ARPE-19 cells, TSPO specific-ligands enhanced the efflux of cholesterol to ApoA-I, apoE and HDL (Fig. 2) and markedly decreased the total cholesterol level, and the biogenesis of free cholesterol (Fig. 3). Equally, TSPO ligand treatment significantly increased expression of ABCA1, ABCG1 and LXRα (Supplementary Material, Fig. S2). CYP27A1 was localised in human RPE (27) and its expression was significantly increased in RPE cells exposed to TSPO specific ligands FGIN-1-27 or XBD173 (Supplementary Material, Fig. 3). Our data suggested TSPO has similar function in cholesterol efflux in RPE cells possibly through oxyterol activated LXR-mediated upregulation of cholesterol transporter genes and down-regulation of cholesterol biosynthesis.

Apolipoprotein-containing lipoproteins accumulate and become oxidized in drusen (36). Apolipoprotein B100 (apoB100) is the major apolipoprotein of LDL, and oxidized apoB100 and OxLDL localized in drusen (37). Early data showed OxLDL was internalized by RPE cells, causing a defect in outer segment phagocytosis and induced apoptosis (37–40). Recent data demonstrated OxLDL triggered the alternative complement pathway by decreasing complement regulator CD59 and increasing the formation of membrane attack complexes (MACs) in RPE cells (41,42). Our experiments indicated that deletion of TSPO enhance OxLDL uptake and accumulation in RPE cells (Fig. 5), which may contribute to abnormal outer segment phagocytosis and dysfunction of the alternative complement system. Certainly, loss of TSPO caused increased oxidative stress in RPE cells by producing higher level of ROS (Fig. 7A, B) and secretion of IL-1β and TNFα levels was markedly increased in OxLDL-treated TSPO$^{-/-}$ RPE cells (Fig. 7C, D). When ARPE-19 cells were exposed to IL-1β or TNFα, the expression of LDLR was significantly upregulated (Supplementary Material, Fig. S5), which promotes OxLDL uptake. ROS also can oxidatively modify macromolecules such as DNA, protein and lipid and lead to dysfunction of RPE cells. Together, these data suggest that loss of TSPO contributes to both dysregulated cholesterol metabolism and inflammation, and may play a central in the pathogenesis of AMD.

TSPO is upregulated in activated microglial cells of different neurodegenerative diseases and recognized as a biomarker for early diagnosis and disease progression (43); TSPO expression

was significantly increased at mRNA and protein level in retinal microglial cells by LPS-induced inflammation (23,25). TSPO was also strongly upregulated in retinal microglia in models of retinal injury and degeneration (23,25). Knockdown of TSPO significantly increased ROS production and TNFα secretion in microglial cells (BV2) in response to LPS challenge; there was no significant increase of ROS production and TNFα expression in knockdown cells without LPS-activation, possibly due to only 30–40% TSPO depletion (23). In this study, TSPO knockout RPE cells had significant increase in the production of ROS and in secretion of IL-1β and TNFα (Fig. 7C, D). TSPO ligand (PK-11195 and Ro5-4864) treatment significantly decreased ROS production and TNFα secretion in BV2 cells; intravitreal treatment with a TSPO ligand (TTN) inhibited LPS-induced retinal inflammatory reaction by reducing retinal lipid peroxidation and TNFα protein level (25). Treatment with another TSPO ligand, XBD173, reduced expression of pro-inflammatory genes and prevented photoreceptor cell death in light-induced retinal degeneration (44). We also found treatment with TSPO ligands significantly down-regulated expression of pro-inflammatory cytokines in ARPE-19 cells (data not shown).

Previous reports showed that TSPO was localized to retinal microglia and inner retinal blood vessels (23,25). We found very strong TSPO signal in three-month old mouse RPE cells, less strong signal in the choroid and some weak signals in the inner and outer plexiform layers (possibly the microglia); we also found quite strong signals in ganglion cells (Fig. 8A, B). Ishikawa *et al.* reported that increased pressure could upregulate TSPO expression in rat ganglion cells; TSPO was undetectable at 10 mmHg and significantly increased in ganglion cells at 35 mmHg and 75 mmHg respectively (45). The difference of immunolocalization of TSPO in retina was possibly due to different approaches for preparing immunostaining samples or immunodetection methods. We used qRT-PCR and Western blotting to confirmed higher level of TSPO expression RPE/choroid when compared to the retina (Fig. 8C–E). During retinal development, Wang *et al.* detected highest TSPO mRNA level in postnatal 0 (P0) retina, then significantly lower but steadily increased in postnatal age (P0–P28), TSPO protein was also steadily increased in postnatal age (P0–P28) (25). However, another group found TSPO mRNA was at highest level in P3 retina then continuously decreased to low levels in adult (P60) retinas (23). We found that TSPO expression was markedly decreased in aged mouse retina and RPE/choroid (Fig. 9A–C, Supplementary Material, Fig. S6B). Aged mouse RPE cells had lower level of cholesterol efflux and higher level of total cholesterol (Fig. 9D, E), which may be in part due to decreased TSPO, which appears to regulate cholesterol efflux in the RPE cells (Fig. 2 and Supplementary Material, Fig. S4).

Prevention of AMD progression is a priority in the long-term care of patients with early stage disease. In pursuit of this objective several strategies are currently being investigated including high-dose lipid lowering therapy (46) and laser-based interventions (47). Targeting the cholesterol efflux pathway in order to ameliorate and/or reverse subretinal accumulation of lipid with associated RPE dysfunction warrants further investigation. The availability of an approved TPSO ligand therapeutic paves the way for translation to clinical trial. If safety and efficacy are demonstrated this novel approach would usefully impact a key pathway likely to be involved in the complex process of progression from early to late stage AMD. How modification of the TPSO pathway using a biochemical approach or AAV-gene therapy might supplant or supplement other tools in reducing the burden of AMD-related visual loss requires further study. Further we plan to investigate the role of this pathway in other conditions which show sub-retinal deposits resembling AMD for example late-onset retinal degeneration (48) and Sorsby fundus dystrophy (49).

Materials and Methods

Reagents

Cell culture medium, trysin and penicillin/streptomycin were purchased from Lonza, UK. Lipofectamine 2000 Transfection reagent, T-PER Tissue Protein Extraction, and Amplex® Red Cholesterol Assay were from Thermo Fisher Scientific, UK. ApoE, ApoA-I, HDL and LDL were purchased from the Athens Research (USA). Oxidized LDL (oxLDL) and fluorescence-labelled oxidized LDL (Dil-acLDL) were purchased from Alfa Aesar, UK. Recombinant human TNFα, IL-Iβ and human TNF-α and IL-Iβ ELISA Development Kit were from Peprotech, UK. Radiochemicals ([^{3}H]cholesterol and [^{14}C]acetic acid) and Scintilant were provided by the ICN Biologicals. G418, TLC plate, phospholipids Assay, dispase II protease, Tri Reagent and tetrazolium salt were purchased from Sigma–Aldrich. Cas9 vector and gRNA vector were obtained from Addgene, USA. Antibodies, TSPO (ab109497), CYP27A1 (Ab64889), LXRα (ab176323), ABCA1 (ab7360), ABCG1 (ab52617), Alexa fluo 594 conjugated secondary antibody and GAPDH antibody were from Abcam. CYP46A1 and LDLR antibodies were from Novus Biologicals, UK. Donkey anti mouse and donkey anti rabbit secondary antibodies were from Santa Cruz, UK. Mito ViewTM Green was from Biotium, UK.

Cell culture

The human retinal pigment epithelium cell line (ARPE-19, ATCC® CRL-2302™) were maintained in DMEM/F-12 medium supplemented with 10% (v/v) fetal bovine serum (FBS), penicillin/streptomycin (50 μg/ml and 50 IU/ml respectively) and 0.26% Sodium bicarbonate. For experiments, cells were grown on to 48, 24, 12 and 6-well plates at density of 1×10^5, 2×10^5, 4×10^5 and 8×10^5 cells per well respectively.

Cells viability

The ARPE-19 cells (1×10^5 cells/well) were cultured in 48-well plates. The cells were treated with different TSPO ligands (FGIN-1-27, XBD173, Etifoxine) in serum free media and incubated for 24 h. Then the cells were washed with PBS and treated with serum-free medium containing 0.4 mg/ml MTT[3-(4, 5-dimethylthiazol-2-l)-2,5-diphenyltetrazolium bromide]. During this period of treatment, mitochondrial cytosolic dehydrogenases of living cells reduced the yellow tetrazolium salt (MTT) to a purple formazan dye suitable for spectrophotometric detection. After 2 h the MTT solution was aspirated and dimethylsulfoxide (0.2 ml/well) was added to dissolve the formazan. The plate was shaken for 10 min and then was read on a micro plate reader (EPOCH) at 575 nm for densities. The absorbance was normalized to untreated cells representing 100% cell viability.

Measurement of [^{3}H]cholesterol efflux

Efflux of [^{3}H]cholesterol to apoAI, apoE, HDL and human serum (HS) in RPE cells was determined following previous description (8). Briefly, cells were seeded on 12 well plates and labelled with [^{3}H]cholesterol for 24 h with 2% BSA in serum free culture media. Efflux was initiated by the addition of serum-free DMEM/

F12 containing human apoAI (10 μg/ml), apoE (10 μg/ml), HDL (20 μg/ml) or human serum (1%, v/v) and in the presence or absence TSPO ligands, and cultured for 24 h. Cholesterol efflux was then calculated as an expression of percentage of cholesterol efflux to each of the acceptors as follows: % efflux = (disintegrations per minute (DPM) media/DPM Media + DPM Cells) × 100.

Lipid analysis

Incorporation of [^{14}C]acetic acid (1 μCi/ml) into fatty acid, phospholipid, cholesterol, cholesteryl ester and triacylglycerol pools was measured after incubation in the presence or absence of TSPO ligands for 24 h, as previously described (8). Cellular lipids were extracted using hexane:isopropanol (3:2, v/v), dried under nitrogen gas and resuspended in isopropanol, before separation by thin-layer chromatography (TLC) using mobile phase-I buffer (chloroform, methanol and water, 60:30:5, v/v/v) and mobile phase-II buffer (hexane, diethyl ether and andacetic acid, 80:20:1.5, v/v/v). Lipids were identified by co-migration with authentic standards and incorporation of radiolabel assessed by scintillation counting. Mass of total cellular cholesterol and phospholipids in ARPE-19 cells was measured using an Amplex® Red Cholesterol Assay Kit (Thermo Fisher scientific) according to the manufacturer's guidance. Total cholesterol mass of mouse RPE/choroid was measured similarly.

Measurement of reactive oxygen species (ROS)

Wildtype and TSPO$^{-/-}$ ARPE-19 cells were incubated with OxLDL (200 μg/ml) for 4 or 24 h. To detect intracellular ROS, cells were incubated for 30 min with the fluorescence dye carboxy-2′,7′-dichloro-dihydro-fluorescein diacetate (DCFHDA, Sigma, UK). The fluorescence signals were measured at 485 (excitation) and 520 nm (emission) using FluoStar Optima MBG-Labtech microplate reader. The ROS level was represented as fluorescence of treated cells)/fluorescence of untreated cells.

Enzyme-linked immunosorbent assay (ELISA)

The cells were treated with oxLDL (200 μg/ml) for 4 or 24 h. The levels of IL-1β and TNF-α in culture medium were quantified by ELISA with human TNF-α and IL-1β kits (Peprotech, UK) following the manufacturer's protocols.

Uptake of oxidized LDL by RPE cells

Fluorescence-labelled DiI-oxidized LDL (DiI-OxLDL) was purchased from Alfa Aesar, UK. ARPE-19 cells were seeded in 6-well plates and treated with DiI-OxLDL (20 μg/ml) for 4 or 24 h. The treated cells were washed five times with PBS and fixed with 4% PFA for 10 min at room temperature then mounted with Vectashield medium with DAPI (Vector Lab Ltd., Peterborough, UK). The intracellular fluorescence-labelled DiI-OxLDL was visualized by LSM 510 Zeiss confocal microscope (Zeiss) and quantified using Image J.

Flow cytometry

The ARPE-19 cells were treated with DiI–labeled oxidized LDL (20 μg/ml) for 4 and 24 h. Then the cells were washed 3 times with PBS and twice with PBS containing BSA (2 mg/ml). The cells were collected by detachment in trypsin, resuspended with complete medium and centrifuged at 1000 rpm for 5 min and washed two times with PBS. The cells were analyzed by flow cytometry (10 000 events; Excitation, 514 nm; Emission; 550 nm) using a FACSCalibur BD Immunocytometry Systems. The data were analyzed by FlowJo software (Treestar Inc).

Knockout of TSPO in ARPE-19 cells

The clustered regularly interspaced short palindromic repeats (CRISPR) system was employed to knockout the TSPO gene from ARPE-19 cells. The CRISP primers were designed using https://benchling.com website to targeting exon 2 of TSPO gene (Accession: NC_018933). The CRISP Oligos were extended using Phusion DNA polymerase (New England Biolab, UK) and ligated into linearized gRNA vector (Addgene 41824) using Gibson assembly to generate a CRISP TSPO-gRNA construct, which was confirmed by sequencing. The CRISP TSPO-gRNA construct and Cas9 plasmid (Addgene 41815) were transfected into ARPE-19 cells. TSPO knockout colonies were verified by Western blotting, Sanger sequencing and immunocytochemistry.

Isolation of primary retinal pigment epithelium (RPE) cells from mouse eyes

Eyes from 3-month and 20-month old mice were washed three times in PBS then washed twice in DMEM F-12 medium. The eyes were transferred into HBSS solution and a circular incision was made around the ora serrata of each eye. The lens and retina were removed, the RPE/choroid/sclera was incubated with 2% dispase solution (w/v) in complete medium for 45 min at 37 °C with 5% CO_2. The RPE/choroid/sclera was washed with PBS twice then incubated with trypsin-EDTA at 37 °C for 15–20 min. After incubation the RPE/choroid/sclera was vigorously shaken to detach the RPE cells. The detached RPE cells were cultured in DMEM F-12 medium until they reached confluent.

Quantitative real-time polymerase chain reaction (qRT-PCR)

Total RNA was extracted from ARPE-19 cells, mouse RPE/choroid, or mouse retinas using Tri Reagent (Sigma, UK) according to the manufacturer's guidance. The cDNA was synthesized by using High Capacity cDNA Reverse Transcription Kit with RNAase inhibitor (Applied Biosystems, UK). The quantification of gene expression was performed by a qRT-PCR assay using a Platinum Syber Green QAPCR Super Mix-UDG w/ROX kit (Invitrigen, UK) with primers for targeted genes.

Immunocytochemistry and immunohistology

Wildtype and TSPO-deleted ARPE-19 cells were incubated with mitochondrial dye, MitoView Green (100 nM, Biotium, USA) in culture medium for 30 min at 37 °C. After multiple washes with PBS, the cells were fixed with 4% paraformaldehyde and blocked with 2% sheep serum with 2% BSA in PBS then stained with a primary rabbit monoclonal TSPO antibody (Abcam ab109497, 1:200 dilution) which recognizes human TSPO C-terminal, and with secondary Alexa Fluor 594 secondary antibody. In addition, mouse (three-month old) eyes were fixed with 4% paraformaldehyde in PBS and cryoprotected in Cryomatrix medium (VWR, UK). The eyes were sectioned and mounted on superfrost slides. The sections were blocked with 2% BSA in PBS and incubated

with primary and secondary antibodies. Images were captured using a LSM 510 confocal microscope (Zeiss).

Western blotting

Cell lysates were prepared in Radio-Immuno Precipitation Assay (RIPA) cell lysis buffer containing 25 mM Tris-HCl pH8, 150 mM Sodium Chloride, 1% (w/v) sodium deoxycholate, 1% (v/v) nonylphenoxypolyethoxylethanol (NP-40) and 0.1% (w/v) sodium dodecyl sulphate supplemented with Complete™ protease inhibitors (Roche). Mouse retina and RPE/choroid tissues were lysed using T-PER™ tissue protein extraction reagent (Thermo Fisher Scientific, UK). Proteins were separated by SDS-PAGE and transferred to nitrocellulose membranes. Target proteins were detected by incubation with primary (1:2000 for TSPO and GAPDH; 1:200 for ABCA1, 1:1000 for ABCG1, CYP27A1 and CYP46A1) and secondary (1:10 000 dilution) antibodies. The intensity of specific bands was quantified using Li-cor Odyssey FC and Image Studio software.

Statistical analysis

Data was analyzed by statistical significance using analysis of variance (ANOVA) and a *t*-test, followed by appropriate post hoc tests (Bonferroni). As indicated, all data are presented as mean ± SD and collected from three independent experiments. Statistical analysis was performed using Prism software (version 6.0 from GraphPad Software Inc., San Diego, CA, USA); $^{*}P < 0.05$, $^{**}P < 0.01$ and $^{***}P < 0.001$, $^{****}P < 0.0001$.

Supplementary Material

Supplementary Material is available at *HMG* online.

Acknowledgements

We would like to thank the Rosetrees Trust, the Glasgow Children's Hospital Charity, the Fight for Sight, Eye Research Fund (Edinburgh and Lothian Health Foundation, ELHF), and the Visual Research Trust for supporting this work.

Conflict of Interest statement. None declared.

References

1. Friedman, D.S., O'Colmain, B.J., Muñoz, B., Tomany, S.C., McCarty, C., de Jong, P.T., Nemesure, B., Mitchell, P. and Kempen, J. Eye Diseases Prevalence Research Group(2004) Prevalence of age-related macular degeneration in the United States. *Arch. Ophthalmol.*, **122**, 564–572.
2. Abdelsalam, A., Del Priore, L. and Zarbin, M.A. (1999) Drusen in age-related macular degeneration: pathogenesis, natural course, and laser photocoagulation-induced regression. *Surv. Ophthalmol.*, **44**, 1–29.
3. Guymer, R., Luthert, P. and Bird, A. (1999) Changes in Bruch's membrane and related structures with age. *Prog. Retin. Eye Res.*, **18**, 59–90.
4. Curcio, C.A., Presley, J.B., Malek, G., Medeiros, N.E., Avery, D.V. and Kruth, H.S. (2005) Esterified and unesterified cholesterol in drusen and basal deposits of eyes with age-related maculopathy. *Exp. Eye Res.*, **81**, 731–741.
5. Neale, B.M., Fagerness, J., Reynolds, R., Sobrin, L., Parker, M., Raychaudhuri, S., Tan, P.L., Oh, E.C., Merriam, J.E. and Souied, E. (2010) Genome-wide association study of advanced age-related macular degeneration identifies a role of the hepatic lipase gene (LIPC). *Proc. Natl. Acad. Sci. USA*, **107**, 7395–7400.
6. Chen, W., Stambolian, D., Edwards, A.O., Branham, K.E., Othman, M., Jakobsdottir, J., Tosakulwong, N., Pericak-Vance, M.A., Campochiaro, P.A., Klein, M.L. *et al.* (2010) Genetic variants near TIMP3 and high-density lipoprotein-associated loci influence susceptibility to age-related macular degeneration. *Proc. Natl. Acad. Sci. USA*, **107**, 7401–7406.
7. Ikonen, E. (2006) Mechanisms for cellular cholesterol transport: defects and human disease. *Physiol. Rev.*, (2006) **86**, 1237–1261.
8. Taylor, J.M., Allen, A.M. and Graham, A. (2014) Targeting mitochondrial 18 kDa translocator protein (TSPO) regulates macrophage cholesterol efflux and lipid phenotype. *Clin. Sci. (Lond.)*, **127**, 603–613.
9. Papadopoulos, V., Aghazadeh, Y., Fan, J., Campioli, E., Zirkin, B. and Midzak, A. (2015) Translocator protein-mediated pharmacology of cholesterol transport and steroidogenesis. *Mol. Cell Endocrinol.*, **408**, 90–98.
10. Fan, J., Campioli, E., Midzak, A., Culty, M. and Papadopoulos, V. (2015) Conditional steroidogenic cell-targeted deletion of TSPO unveils a crucial role in viability and hormone-dependent steroid formation. *Proc. Natl. Acad. Sci. USA*, **112**, 7261–7266.
11. Morohaku, K., Pelton, S.H., Daugherty, D.J., Butler, W.R., Deng, W. and Selvaraj, V. (2014) Translocator protein/peripheral benzodiazepine receptor is not required for steroid hormone biosynthesis. *Endocrinology*, **155**, 89–97.
12. Tu, L.N., Morohaku, K., Manna, P.R., Pelton, S.H., Butler, W.R., Stocco, D.M. and Selvaraj, V. (2014) Peripheral benzodiazepine receptor/translocator protein global knock-out mice are viable with no effects on steroid hormone biosynthesis. *J. Biol. Chem.*, **289**, 27444–22454.
13. Ishida, B.Y., Duncan, K.G., Bailey, K.R., Kane, J.P. and Schwartz, D.M. (2006) High density lipoprotein-mediated lipid efflux from retinal pigmented epithelial cells in culture. *Br. J. Ophthalmol.*, **90**, 616–620.
14. Lakkaraju, A., Finnemann, S.C. and Rodriguez-Boulan, E. (2007) The lipofuscin fluorophore A2E perturbs cholesterol metabolism in retinal pigment epithelial cells. *Proc. Natl. Acad. Sci. USA*, **104**, 11026–11031.
15. Feeney-Burns, L., Hilderbrand, E.S. and Eldridge, S. (1984) Aging human RPE: morphometric analysis of macular, equatorial, and peripheral cells. *Invest. Ophthalmol. Vis. Sci.*, **25**, 95–200.
16. Tserentsoodol, N., Gordiyenko, N.V., Pascual, I., Lee, J.W., Fliesler, S.J. and Rodriguez, I.R. (2006) Intraretinal lipid transport is dependent on high density lipoprotein-like particles and class B scavenger receptors. *Mol. Vis.*, **12**, 1319–1333.
17. Zareparsi, S., Buraczynska, M., Branham, K.E., Shah, S., Eng, D., Li, M., Pawar, H., Yashar, B.M., Moroi, S.E., Lichter, P.R. *et al.* (2005) Toll-like receptor 4 variant D299G is associated with susceptibility to age-related macular degeneration. *Hum. Mole. Genet.*, **14**, 1449–1455.
18. Ishida, B.Y., Bailey, K.R., Duncan, K.G., Chalkley, R.J., Burlingame, A.L., Kane, J.P. and Schwartz, D.M. (2004) Regulated expression of apolipoprotein E by human retinal pigment epithelial cells. *J. Lipid Res.*, **45**, 263–271.
19. Li, C.M., Chung, B.H., Presley, J.B., Malek, G., Zhang, X., Dashti, N., Li, L., Chen, J., Bradley, K., Kruth, H.S. *et al.* (2005) Lipoprotein-like particles and cholesteryl esters in human

Bruch's membrane: initial characterization. *Invest. Ophthalmol. Vis. Sci.*, **46**, 2576–2586.
20. Cosenza-Nashat, M., Zhao, M.L., Suh, H.S., Morgan, J., Natividad, R., Morgello, S. and Lee, S.C. (2009) Expression of the translocator protein of 18 kDa by microglia, macrophages and astrocytes based on immunohistochemical localization in abnormal human brain. *Neuropathol. Appl. Neurobiol.*, **35**, 306–328.
21. Falchi, A.M., Battetta, B., Sanna, F., Piludu, M., Sogos, V., Serra, M., Melis, M., Putzolu, M. and Diaz, G. (2007) Intracellular cholesterol changes induced by translocator protein (18 kDa) TSPO/PBR ligands. *Neuropharmacology*, **53**, 318–329.
22. Ji, B., Maeda, J., Sawada, M., Ono, M., Okauchi, T., Inaji, M., Zhang, M.R., Suzuki, K., Ando, K., Staufenbiel, M. *et al.* (2008) Imaging of peripheral benzodiazepine receptor expression as biomarkers of detrimental versus beneficial glial responses in mouse models of Alzheimer's and other CNS pathologies. *J. Neurosci.*, **28**, 12255–12267.
23. Karlstetter, M., Nothdurfter, C., Aslanidis, A., Moeller, K., Horn, F., Scholz, R., Neumann, H., Weber, B.H., Rupprecht, R. and Langmann, T. (2014) Translocator protein (18 kDa) (TSPO) is expressed in reactive retinal microglia and modulates microglial inflammation and phagocytosis. *J. Neuroinflammation*, **11**, 3.
24. Stephenson, D.T., Schober, D.A., Smalstig, E.B., Mincy, R.E., Gehlert, D.R. and Clemens, J.A. (1995) Peripheral benzodiazepine receptors are colocalized with activated microglia following transient global forebrain ischemia in the rat. *J. Neurosci.*, **15**, 5263–5274.
25. Wang, M., Wang, X., Zhao, L., Ma, W., Rodriguez, I.R., Fariss, R.N. and Wong, W.T. (2014) Macroglia-microglia interactions via TSPO signaling regulates microglial activation in the mouse retina. *J. Neurosci.*, **34**, 3793–3806.
26. Tserentsoodol, N., Sztein, J., Campos, M., Gordiyenko, N.V., Fariss, R.N., Lee, J.W., Fliesler, S.J. and Rodriguez, I.R. (2006) Uptake of cholesterol by the retina occurs primarily via a low density lipoprotein receptor-mediated process. *Mol. Vis.*, **12**, 1306–1318.
27. Zheng, W., Reem, R.E., Omarova, S., Huang, S., DiPatre, P.L., Charvet, C.D., Curcio, C.A., Pikuleva, I.A. and Chaum, E. (2012) Spatial distribution of the pathways of cholesterol homeostasis in human retina. *PLoS One*, **7**, e37926.
28. Maiolino, G., Rossitto, G., Caielli, P., Bisogni, V., Rossi, G.P. and Calò, L.A. (2013) The role of oxidized low-density lipoproteins in atherosclerosis: the myths and the facts. *Mediators Inflamm.*, **2013**, 714653.
29. Ma, K.L., Ruan, X.Z., Powis, S.H., Chen, Y., Moorhead, J.F. and Varghese, Z. (2008) Inflammatory stress exacerbates lipid accumulation in hepatic cells and fatty livers of apolipoprotein E knockout mice. *Hepatology*, **48**, 770–781.
30. Ruan, X.Z., Moorhead, J.F., Tao, J.L., Ma, K.L., Wheeler, D.C., Powis, S.H. and Varghese, Z. (2006) Mechanisms of dysregulation of low-density lipoprotein receptor expression in vascular smooth muscle cells by inflammatory cytokines. *Arterioscler. Thromb. Vasc. Biol.*, **26**, 1150–1155.
31. Tu, L.N., Zhao, A.H., Hussein, M., Stocco, D.M. and Selvaraj, V. (2016) Translocator protein (TSPO) affects mitochondrial fatty acid oxidation in steroidogenic cells. *Endocrinology*, **157**, 1110–1121.
32. Pikuleva, I.A. and Curcio, C.A. (2014) Cholesterol in the retina: the best is yet to come. *Prog. Retin. Eye Res.*, **41**, 64–89.
33. Sene, A., Khan, A.A., Cox, D., Nakamura, R.E.I., Santeford, A., Kim, B.M., Sidhu, R.ohini., Onken, M.D., Harbour, J.W., Hagbi-Levi, S. *et al.* (2013) Impaired cholesterol efflux in senescent macrophages promotes age-related macular degeneration. *Cell Metabolism*, **17**, 549–561.
34. Graham, A. (2015) Mitochondrial regulation of macrophage cholesterol homeostasis. *Free Radic. Biol. Med.*, **89**, 982–992.
35. Li, F., Liu, J., Liu, N., Kuhn, L.A., Garavito, R.M. and Ferguson-Miller, S. (2016) Translocator protein 18 kDa (TSPO): an old protein with new functions? *Biochemistry*, **55**, 2821–2831.
36. Curcio, C.A., Johnson, M., Huang, J.D. and Rudolf, M. (2009) Aging, age-related macular degeneration, and the response-to-retention of apolipoprotein B-containing lipoproteins. *Prog. Retin. Eye Res.*, **28**, 393–422.
37. Yamada, Y., Tian, J., Yang, Y., Cutler, R.G., Wu, T., Telljohann, R.S., Mattson, M.P. and Handa, J.T. (2008) Oxidized low density lipoproteins induce a pathologic response by retinal pigmented epithelial cells. *J. Neurochem.*, **105**, 1187–1197.
38. Gordiyenko, N., Campos, M., Lee, J.W., Fariss, R.N., Sztein, J. and Rodriguez, I.R. (2004) RPE cells internalize low-density lipoprotein (LDL) and oxidized LDL (oxLDL) in large quantities in vitro and in vivo. *Invest. Ophthalmol. Vis. Sci.*, **45**, 2822–2829.
39. Hoppe, G., Marmorstein, A.D., Pennock, E.A. and Hoff, H.F. (2001) Oxidized low density lipoprotein-induced inhibition of processing of photoreceptor outer segments by RPE. *Invest. Ophthalmol. Vis. Sci.*, **42**, 2714–2720.
40. Hoppe, G., O'Neil, J., Hoff, H.F. and Sears, J. (2004) Accumulation of oxidized lipid-protein complexes alters phagosome maturation in retinal pigment epithelium. *Cell Mol. Life Sci.*, **61**, 1664–1674.
41. Ebrahimi, K.B., Fijalkowski, N., Cano, M. and Handa, J.T. (2013) Decreased membrane complement regulators in the retinal pigmented epithelium contributes to age-related macular degeneration. *J. Pathol.*, **229**, 729–742.
42. Tan, L.X., Toops, K.A. and Lakkaraju, A. (2016) Protective responses to sublytic complement in the retinal pigment epithelium. *Proc. Natl. Acad. Sci. USA*, **113**, 8789–8794.
43. Dupont, A.C., Largeau, B., Santiago Ribeiro, M.J., Guilloteau, D., Tronel, C. and Arlicot, N. (2017) Translocator protein-18 kDa (TSPO) positron emission tomography (PET) imaging and its clinical impact in neurodegenerative diseases. *Int. J. Mol. Sci.*, **18**, 785.
44. Scholz, R., Caramoy, A., Bhuckory, M.B., Rashid, K., Chen, M., Xu, H., Grimm, C. and Langmann, T. (2015) Targeting translocator protein (18 kDa) (TSPO) dampens pro-inflammatory microglia reactivity in the retina and protects from degeneration. *J. Neuroinflammation*, **12**, 201.
45. Ishikawa, M., Yoshitomi, T., Covey, D.F., Zorumski, C.F. and Izumi, Y. (2016) TSPO activation modulates the effects of high pressure in a rat ex vivo glaucoma model. *Neuropharmacology*, **111**, 142–159.
46. Vavvas, D.G., Daniels, A.B., Kapsala, Z.G., Goldfarb, J.W., Ganotakis, E., Loewenstein, J.I., Young, L.H., Gragoudas, E.S., Eliott, D., Kim, I.K., Tsilimbaris, M.K. and Miller, J.W. (2016) Regression of some high-risk features of age-related macular degeneration (AMD) in patients receiving intensive statin treatment. *EBioMedicine*, **5**, 198–203.
47. Jobling, A.I., Guymer, R.H., Vessey, K.A., Greferath, U., Mills, S.A., Brassington, K.H., Luu, C.D., Aung, K.Z., Trogrlic, L., Plunkett, M. and Fletcher, E.L. (2015) Nanosecond laser

therapy reverses pathologic and molecular changes in age-related macular degeneration without retinal damage. *FASEB J.*, **29**, 696–710.

48. Hayward, C., Shu, X., Cideciyan, A.V., Lennon, A., Barran, P., Zareparsi, S., Sawyer, L., Hendry, G., Dhillon, B. and Milam, A.H. Mutation in a short-chain collagen gene, CTRP5, results in extracellular deposit formation in late-onset retinal degeneration: a genetic model for age-related macular degeneration. *Hum. Mol. Genet.*, **12**, 2657–2667.
49. Gliem, M., Müller, P.L., Mangold, E., Holz, F.G., Bolz, H.J., Stöhr, H., Weber, B.H. and Charbel Issa, P. (2015) Sorsby fundus dystrophy: novel mutations, novel phenotypic characteristics, and treatment outcomes. *Invest. Ophthalmol. Vis. Sci.*, **56**, 2664–2676.